DOI: 10.3901/CJME.2016.0114.008, available online at www.springerlink.com; www.cjmenet.com

# Two Dimensional Nanoscale Reciprocating Sliding Contacts of Textured Surfaces

TONG Ruiting[1, *], LIU Geng[1], and LIU Tianxiang[2]

1 *Shaanxi Engineering Laboratory for Transmissions and Controls, Northwestern Polytechnical University, Xi'an 710072, China*
2 *Institute for Mechanics and Fluid Dynamics, Technische Universit Bergakademie Freiberg, Lampadiusstr. 4, Freiberg 09596, Germany*

Received June 12, 2015; revised December 10, 2015; accepted January 14, 2016

**Abstract:** Detailed behaviors of nanoscale textured surfaces during the reciprocating sliding contacts are still unknown although they are widely used in mechanical components to improve tribological characteristics. The current research of sliding contacts of textured surfaces mainly focuses on the experimental studies, while the cost is too high. Molecular dynamics(MD) simulation is widely used in the studies of nanoscale single-pass sliding contacts, but the CPU cost of MD simulation is also too high to simulate the reciprocating sliding contacts. In this paper, employing multiscale method which couples molecular dynamics simulation and finite element method, two dimensional nanoscale reciprocating sliding contacts of textured surfaces are investigated. Four textured surfaces with different texture shapes are designed, and a rigid cylindrical tip is used to slide on these textured surfaces. For different textured surfaces, average potential energies and average friction forces of the corresponding sliding processes are analyzed. The analyzing results show that "running-in" stages are different for each texture, and steady friction processes are discovered for textured surfaces II, III and IV. Texture shape and sliding direction play important roles in reciprocating sliding contacts, which influence average friction forces greatly. This research can help to design textured surfaces to improve tribological behaviors in nanoscale reciprocating sliding contacts.

**Keywords:** nanoscale, reciprocating sliding contacts, textured surface, multiscale method

## 1 Introduction

Textured surfaces in sliding contacts play important roles in many mechanical components[1–4] as it can improve tribological characteristics. With the development of micro/nanoelectro mechanical systems, the sizes of components come to micro/nano scale, and textures will influence real contact areas to affect the friction process further. MITCHELL, et al[5], investigated single and reciprocating friction behaviors of micropatterned surfaces. For single-pass testing, lower coefficients of friction (COFs) were obtained with larger depression sizes and larger pillar sizes. They also pointed out that the single-pass COF measurements were not good predictions of the steady state COF values measured. The studies of SINGH, et al[6], showed that at both nano- and micro-scales, the modified Si (1 0 0) surfaces exhibited enhanced friction behaviors when compared with bare Si (1 0 0) surfaces. Furthermore, wear was observed in the test samples, which influenced their friction properties. The wear particles are trapped by the texture or act as lubricant, which will further influence the sequent sliding process. Understanding detailed behaviors of textured surfaces during the reciprocating sliding contacts will help to achieve desired friction characteristics.

Great efforts have been made to investigate the effects of textured surfaces on friction properties in reciprocating sliding contacts. MENEZES, et al[7], used pins made of Al-4Mg alloys to slide against steel plates at various numbers of cycles through a pin-on-plate reciprocating sliding tester. Three different surface textures including unidirectional, 8-ground, and random were created on the plates. For the unidirectional and 8-ground textures, COFs decreased with the number of cycles, while the random texture showed opposite trend. Choosing stainless steel AISI 416 pin, pin-on-plate reciprocating tests on tribological behaviors of laser-textured NiCrBSi coatings were performed by GARRIDO, et al[8]. The results showed that textured surfaces with smaller dimple diameters could improve the tribological behaviors. Incorrect dimple density values led to disruptive behaviors due to both high and low dimple ratios. CHOUQUET, et al[9], made cavities on a DLC layer and investigated the tribological properties of the DLC/steel lubricated sliding contact by using a ball-on-disk apparatus. They found that the DLC layer with small and shallow cavities allowed a significant reduction of COF of a DLC/steel contact compared with a system with non-textured DLC film. Furthermore, wear rates of the

* Corresponding author. E-mail: tongruiting@nwpu.edu.cn
Supported by National Natural Science Foundation of China (Grant Nos. 51205313, 50975232), Fundamental Research Funds for the Central Universities of China (Grant No. 3102014JCS05009), and the 111 Project of China (Grant No. B13044)

steel balls were significantly reduced in case of balls used as mating materials against textured DLC coating compared with the ball used against the reference non-textured coating. DENG, et al[10], made micro-holes on the surface of WC/TiC/Co carbide tool. Reciprocating sliding tests and dry cutting tests were carried out with the carbide tool. Compared with non-textured surfaces, the tool with textured surface showed a great decrease in cutting forces and COFs at the tool-chip interface for the case of low speed cutting, while for high speed the difference was light. PODGORNIK, et al[11], investigated the role of textured surfaces under different lubrication regimes by combining experimental and numerical analysis. For starved lubrication, textured surfaces resisted sliding and resulted in increased friction. In boundary lubrication, textured surfaces with smaller dimples and lower dimple densities led to reduced levels of friction. When approaching to full-film lubrication, textured surfaces with the largest dimple depth showed less friction. RAMESH, et al[12], performed experimental and numerical investigations on friction characteristics of microtextured surfaces. Under hydrodynamic lubricated reciprocating sliding conditions, the friction of textured surfaces showed as much as 80% lower than the untextured surfaces. The investigation of KOVALCHENKO, et al[13] found that although laser surface texturing(LST) provided tribological benefits in terms of friction reduction in conformal and relatively low-pressure lubricated contacts, the LST increased wear of the counterface for the case of non-conformal and relatively high-pressure lubricated reciprocating sliding contacts. ACHANTA, et al[14], carried out reciprocating sliding tests with a modular microtribometer to study friction and nanowear of hard coatings. They discovered that wear particles were filled into the spacings between asperities. Therefore, the structure and distribution of asperities played key roles in affecting local stresses and thereby friction and wear resistance. PETTERSSON, et al[15], created parallel grooves and crossed grooves with different spacings on the piston surfaces. Reciprocating sliding tests showed that all the textures could obtain lower COFs at the initial stage, while the difference between COFs became little soon. The experimental studies obtained so many valuable results in spite of high cost for equipments or samples. Numerical approaches can help to discover the underlying phenomena in the contacting bodies and save the experimental cost, which become more and more important.

From the experimental literatures above, we can see that parameters of textured surfaces[7–9, 11], sliding speed[10], lubricating conditions[11–12], applied load[13], wear particles[14] or cycle numbers[15] all influence the reciprocating sliding processes. For numerical studies, molecular dynamics(MD) simulations were widely used in the studies of nanoscale single-pass sliding contacts, and lots of factors were also found to influence the sliding processes. In many numerical simulations, surface roughness influenced friction characteristics dramatically[16–20], which indicated that textured surfaces would always affect the sliding process by changing surface roughness. Besides, some other factors, such as indentation depth[21–22], temperature[23], sliding velocity[22–23], tip radius[22, 24], sliding direction[19, 25], applied load[19, 23] all contributed to the sliding process, which agreed with the experimental results. Furthermore, chips were discovered in Ref. [21] due to atoms near the interface accumulated in front of the slider. According to Ref. [26], the contribution of the chip could not be neglected. Textured surfaces can trap the chip to further influence the consequent sliding process. Moreover, rough surfaces become flat rapidly due to repetitive sliding[16], which indicated that reciprocating sliding contacts were quite different from single-pass sliding contacts. However, there are few studies on the reciprocating sliding contacts of textured surfaces by numerical methods due to extremely high cost of CPU time. A hybrid method[27] which could save much computation time was applied to two dimensional nanoscale contact problems, and the similar methods were used to study two dimensional nanoscale sliding contacts[22] or nanoscratching problems[28], which showed the applicability of these methods. Therefore, in this work, we will introduce the hybrid method to the simulation of reciprocating sliding contacts of textured surfaces.

Employing multiscale method which couples molecular dynamics simulation and finite element method, two dimensional nanoscale reciprocating sliding contacts of textured surfaces are investigated in this paper. Four textured surfaces with different texture shapes are designed, and a rigid cylindrical tip is used to slide on these textured surfaces. Average potential energies and average friction forces of each sliding process are analyzed. The effects of textured surfaces on the “running-in” stages and steady state are discussed.

## 2 Model Descriptions

As shown in Fig. 1, a multiscale model is used to investigate two dimensional nanoscale reciprocating sliding contacts between a rigid cylindrical tip and textured surfaces. The rigid cylindrical tip consists of 4 layers with 120 atoms, and its radius is $R=30r_0$ ($r_0$ is the Lennard-Jones parameter, $r_0=0.227\ 7$ nm[29] here). The substrate is divided to two parts: MD region and finite element (FE) region. For the MD region, there are 31 layers in $y$ direction and 113 atoms per layer in $x$ direction besides the textures. Defining the distance between two adjacent atoms is $d_x$ ($d_x=2^{1/6}r_0$) in $x$ direction, and $d_y$ ($d_y=3^{1/2}/2\times d_x$) represents the distance between two adjacent layers in $y$ direction, the dimension of the MD region is $112.5d_x\times 30.0d_y$. Triangular finite elements are used to discretize the FE region, and there are 102 nodes and 162 elements totally. The dimension of the FE region is $112.5d_x\times 56.0d_y$, and the overlap region between the MD region and the FE region is $112.5d_x\times 6.0d_y$. Therefore, the dimension of the whole model is

$112.5d_x \times 80.0d_y$ (corresponding to 113 atoms/layer×81 layers for full MD model). Initial gap between the tip and substrate is $d_g=2.5r_0$. Textures on the substrate are named as the "1st texture", "2nd texture", …, "7th texture".

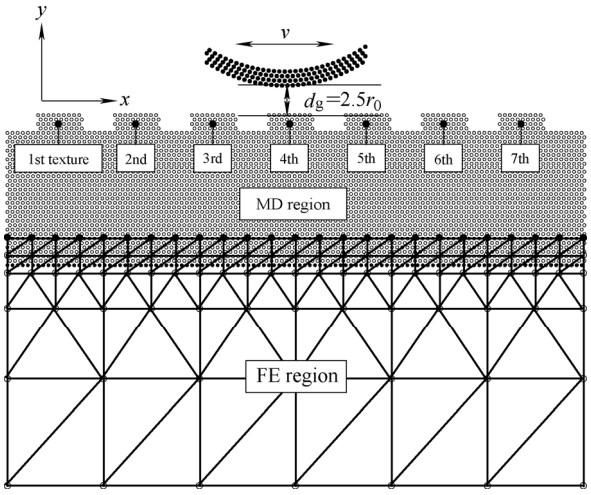


Fig. 1. Nanoscale reciprocating sliding contact model between a rigid cylindrical tip and a textured surface

Four textured surfaces are designed in this paper. The parameters of the textured surfaces in this work are designed as width $a=8d_x$, spacing $b=7d_x$, and height as $h=4d_y$. The four textured surfaces are shown in Fig. 2 with different texture shapes, and named as surface I, II, III and IV, respectively. For surface I, the number of atoms in each layer of a single texture is, $m_A=9$. For surface II, the number of atoms from bottom layer to top layer of each single texture is changed from, $m_A=9$, to 8, 7 and 6, etc. The numbers are 9, 9, 8 and 8 for the textures of surfaces III and IV. The number of textures for these four textured surfaces is $n_A=7$.

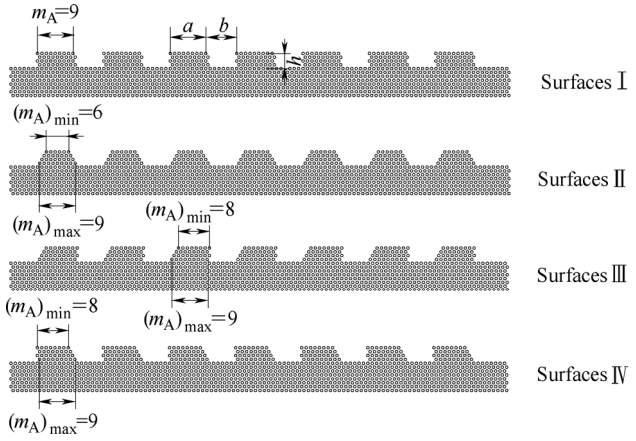


Fig. 2. Topographies of textured surfaces

Multiscale method[27] is used to simulate this reciprocating sliding contact problem. Lennard-Jones (L-J) potential is employed to describe interactions between all the atoms:

$$U(r_{ij})=4\varepsilon\left[\left(\frac{r_0}{r_{ij}}\right)^{12}-\left(\frac{r_0}{r_{ij}}\right)^{6}\right],\quad r_{ij}\leqslant r_c, \tag{1}$$

where $r_{ij}=\left\|\boldsymbol{r}_i-\boldsymbol{r}_j\right\|$, denotes the distance between atoms i and j, $\varepsilon$ and $r_0$ are the L-J parameters. For FCC Cu, $\varepsilon=6.648\times10^{-20}$ J, $r_0=0.227\ 7$ nm[29]. The relationships between the reduced units and the Systeme International (SI) units used in this paper are same as Ref. [22]. The cut-off radius, $r_c=2.2r_0$ according to Ref. [30] here. Fixed boundary conditions are applied along the left and right boundaries of the MD region. The force that atom j exerts on atom i can be obtained as follows:

$$\boldsymbol{F}(r_{ij})=-\nabla U(r_{ij})=\left(\frac{48\varepsilon}{r_0^{\,2}}\right)\left[\left(\frac{r_0}{r_{ij}}\right)^{14}-\frac{1}{2}\left(\frac{r_0}{r_{ij}}\right)^{8}\right]\boldsymbol{r}_{ij},\ r_{ij}\leqslant r_c. \tag{2}$$

Velocity-Verlet algorithm[31] is used to calculate coordinates, velocities, and accelerations of all the atoms:

$$\begin{cases}\boldsymbol{r}(t+\Delta t)=\boldsymbol{r}(t)+\boldsymbol{v}(t)\Delta t+\dfrac{1}{2}\boldsymbol{a}(t)\Delta t^2,\\ \boldsymbol{v}\left(t+\dfrac{\Delta t}{2}\right)=\boldsymbol{v}(t)+\dfrac{1}{2}\boldsymbol{a}(t)\Delta t,\\ \boldsymbol{a}(t+\Delta t)=-\dfrac{1}{m}\nabla U(\boldsymbol{r}(t+\Delta t)),\\ \boldsymbol{v}(t+\Delta t)=\boldsymbol{v}\left(t+\dfrac{\Delta t}{2}\right)+\dfrac{1}{2}\boldsymbol{a}(t+\Delta t)\Delta t,\end{cases} \tag{3}$$

where $\Delta t$ is time step, $\boldsymbol{r}$ is coordinate vector, $\boldsymbol{v}$ is velocity vector, $\boldsymbol{a}$ is acceleration vector, and $m$ is mass of an atom.

FE calculations are carried out through linear triangular elements. Considering that displacement of the FE region is very small comparing with those in the MD region, quasi-static elastic constitutive relationship and Newton-Raphs on iteration are employed during calculations of the FE region. The coupling process is achieved through the overlap region. MD region is relaxed to reach its minimum energy configuration. After the relaxation, FE calculations will take on once when MD takes on 50 time steps, and the displacements of FE nodes are calculated through the displacements of atoms around them. According to the positions of atoms on the bottom and the displacements of FE nodes, the displacements of the bottom atoms can be obtained by FE interpolation. Then, a new MD model whose atoms positions are relocated is achieved, and one can repeat the process above to perform the multiscale method.

## 3 Results and Discussion

For MD simulations in this paper, velocity-Verlet algorithm is carried out with a fixed time step, $\Delta t=0.95$ fs. Initially, velocities of atoms except fixed boundary ones are set with random Gaussian distribution under an equivalent temperature $T=300$ K. Before loading, the system is relaxed to reach its minimum energy configuration. Then, the tip moves to the substrate with a displacement

increment $\Delta s = 0.05r_0$ and indentation speed keeps at $v$=2.0 m/s in $y$ direction. The indentation depth is $d$=2.5$r_0$. As the indentation finishes, the tip slides along $x$ direction, and sliding speed is also $v$=2.0 m/s. According to Ref. [32], high sliding speed may induce biased results, so the sliding speed is chosen as $v$=2.0 m/s here. The tip moves to the right (forward sliding, corresponding to odd sliding numbers) for 320Δ$s$, and then it moves to the left (backward sliding, corresponding to even sliding numbers) for 320Δ$s$. The forward and backward sliding processes are carried out for 10 times.

### 3.1 Reciprocating sliding contacts between the tip and surface I

For surface I, Fig. 3 gives average potential energies and average friction forces corresponding to every sliding process. The average potential energies do not reach stable values during the whole sliding process, and the average friction forces do not show stable values either. According to the video of the sliding process of surface I, one can find that atoms on the surface of the substrate are moved by the tip all the time, and the profile of the current surface I does not keep stable, which indicate that the sliding contacts between the tip and surface I still stay at "running-in" stage. During the sliding processes, atoms of the substrate are scratched by the tip or adhere to the tip, and then they are accumulated together or fracture occurs accompanied by accumulation or release of energies, which result in fluctuations of the average potential energies.

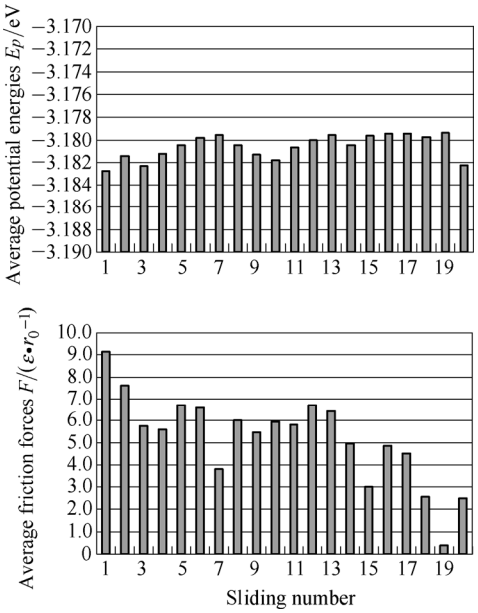


Fig. 3. Average potential energies and average friction forces for every sliding process (surface I)

If one does not consider textures on the substrate, friction force can be written as[33]:

$$F = F_{\text{ploughing}} + F_{\text{adhesion}}, \tag{4}$$

where $F$ is total friction force. $F_{\text{ploughing}}$ and $F_{\text{adhesion}}$ are ploughing component and adhesion component, respectively. Considering the textures on the substrate in this work, attractive forces from the textures which do not contact with the tip are acting on the tip, and the friction force can be rewritten as:

$$F = F_{\text{ploughing}} + F_{\text{adhesion}} + F_{\text{attracting}}, \tag{5}$$

where $F_{\text{attracting}}$ is attracting component. Furthermore, due to the scratch between the tip and textures, chip component $F_{\text{chip}}$ should also be considered[26], and the friction force is finally written as:

$$F = F_{\text{ploughing}} + F_{\text{adhesion}} + F_{\text{attracting}} + F_{\text{chip}}. \tag{6}$$

When the 3rd sliding process finishes, a big texture composed of two layers atoms is formed on the substrate, and one layer atoms adhere to the surface of the tip. During the following sliding processes, the tip takes some atoms to slide on the big texture, and scratches also occur. Therefore, the four components in Eq. (6) attribute to the total friction force at the same time to make the variation of every sliding process. Some atoms accumulate on the 6th texture gradually, and $F_{\text{attracting}}$ mainly comes from the 6th texture. When the 18th sliding process finishes, atoms accumulated on the 6th texture are more than the other sliding process. As the 19th sliding process going on, $F_{\text{attracting}}$ acts in the same direction as the sliding direction, and more atoms results in higher $F_{\text{attracting}}$. That is why the average friction force of the 19th sliding process shows the lowest value. For the 20th sliding process, $F_{\text{attracting}}$ from the 6th texture gets opposite direction to the sliding direction, and the average friction force increase to higher value.

It is interesting to note that the average friction forces have a trend that they decrease as sliding numbers increase although they fluctuate in these 20 sliding processes. During all these sliding processes, the 4th and 5th textures are scratched and flattened by the tip, so the ploughing component $F_{\text{ploughing}}$ becomes lower as the sliding going on. Besides, atoms of the textures are scratched to fill into the spacings, which makes the chip component $F_{\text{chip}}$ also decrease gradually.

### 3.2 Reciprocating sliding contacts between the tip and surface II

Fig. 4 shows average potential energies and average friction forces for the case of reciprocating sliding contacts between the tip and surface II. Average friction forces in the steady state are quite different from the cases of "running-in" stage, which is similar to Ref. [5]. Besides, the phenomenon agrees with the traditional friction trends. According the video of the sliding processes, stable surface structure is formed after the 10th sliding process. From the 11th sliding process, the tip takes some atoms to slide smoothly on a big texture formed by atoms of original textures, and the average potential energies are stable.

Atoms do not accumulate on the 6th texture due to that one single texture of surface II gets fewer atoms than surface I. Therefore, attracting component $F_{\text{attracting}}$ from the 6th texture is small and its contribution to the total friction force is slight. Besides, the ploughing component, $F_{\text{ploughing}}=0$, and the chip component, $F_{\text{chip}}=0$ due to smooth sliding contacts after the 10th sliding process. Adhesion component $F_{\text{adhesion}}$ is the main contributor to the total friction force during the stable sliding stages.

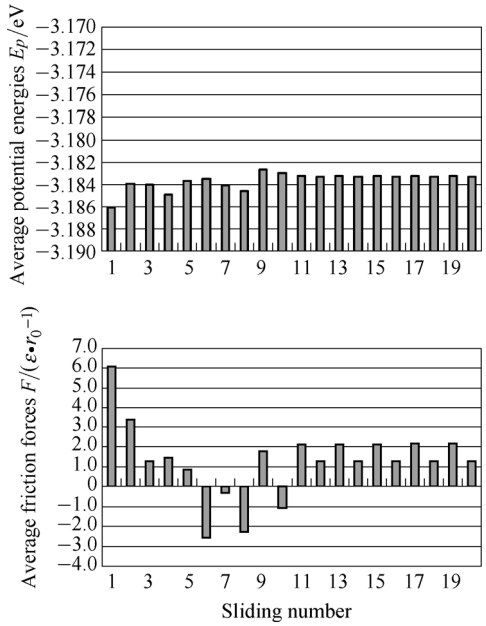


Fig. 4. Average potential energies and average friction forces for every sliding process (surface II)

Atoms of one single texture of surface II are so few that the spacing between the 4th and 5th textures can not be filled to form a big flat texture. The big texture can be divided to two parts: left part and right part, and the adhesion component can also be divided to left component $F^{\text{L}}_{\text{adhesion}}$ (adhesive force between the tip and the left part of the big texture) and right component $F^{\text{R}}_{\text{adhesion}}$ (adhesive force between the tip and the right part of the big texture). The left part of the big texture consists of two layers atoms and the right part gets one layer atoms, so $F^{\text{L}}_{\text{adhesion}}$ plays the main role in the total friction force. The direction of $F^{\text{L}}_{\text{adhesion}}$ is opposite to the sliding direction for odd sliding processes (slides to the right), while these two directions are the same for even sliding processes (slides to the left), which are the reasons for the difference between the average friction forces in the steady state. The reciprocating sliding process reaches steady state since the 11th sliding, and the "running-in" stage is shorter than the case of surface I, which can be beneficial to reduce friction.

### 3.3 Reciprocating sliding contacts between the tip and surface III

Fig. 5 gives average potential energies and average friction forces for every sliding process for the case of surface III. From the 13th sliding process, the average potential energies are stable, and the average friction forces fluctuate regularly, which indicate that the sliding contacts come to steady state. It should be noted that, the average friction forces for odd sliding number are lower, while for even sliding number are higher except for the 1st and 2nd sliding process. During the 1st sliding process, the 4th texture is compressed to 3 layers and the tip scratches the 5th texture, which induce large contact area and high ploughing component corresponding to high $F_{\text{adhesion}}$ and $F_{\text{ploughing}}$. Therefore, the average friction force of the 1st sliding process gets a high value. From the 3rd sliding process, the tip takes many atoms from the textures, and few atoms accumulate to form the chip, so the chip component $F_{\text{chip}}$ is small. The current 4th and 5th textures only have two layers, and rare scratch between the tip and textures occurs to result in low ploughing component $F_{\text{ploughing}}$. Attracting component $F_{\text{attracting}}$ and adhesion component $F_{\text{adhesion}}$ play the main roles in the following sliding processes. For odd sliding number, the tip takes atoms to slide to the right, and the direction of $F_{\text{attracting}}$ from the 6th texture is same as the sliding direction, so the average friction forces are lower. On the contrary, the two directions are opposite to each other to make higher average friction forces for the even sliding processes.

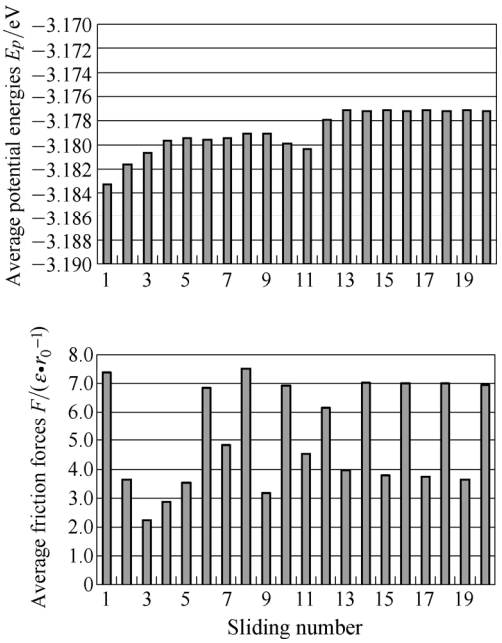


Fig. 5. Average potential energies and average friction forces for every sliding process (surface III)

During the stable sliding processes, the big texture consists of 2 layers atoms and the tip slides smoothly, so the ploughing component, $F_{\text{ploughing}}=0$, and the chip component, $F_{\text{chip}}=0$. The stable average friction forces are reduced slightly compared with the 1st sliding process, and they are higher than the case of surface II, which indicates that surface III is worse than surface II to reduce friction forces in reciprocating sliding contacts.

### 3.4 Reciprocating sliding contacts between the tip and surface IV

The average potential energies and average friction

forces of every sliding process for the case of surface IV are shown in Fig. 6. The "running-in" stage of surface IV only keeps 8 sliding processes, which is shorter than the other cases. The "running-in" stage also indicates that surface IV is better than other cases to reach stable friction state. In the 1st sliding process, the tip takes the 4th texture to slide towards the 5th texture and scratches the 5th texture at the same time. At the end of this sliding process, the 4th texture connects to the 5th texture to form a big texture which contains 3 layers atoms. Combination of high ploughing component $F_{\text{ploughing}}$, high adhesion component $F_{\text{adhesion}}$ and low chip component $F_{\text{chip}}$ results in the highest average friction force. During the following sliding processes, $F_{\text{ploughing}}=0$ due to that the big texture is already formed, and $F_{\text{adhesion}}$ plays the main role. Some atoms of the substrate adhere to the tip and are taken by the tip to slide together. More and more atoms are taken by the tip until the big texture consists of 2 layers, and the sliding processes come to steady state. From the 9th sliding process, the adhesion component $F_{\text{adhesion}}$ and attracting component $F_{\text{attracting}}$ determine the friction forces. For odd sliding processes, the tip takes atoms to slide to the 6th texture, and the atoms taken by the tip connect to the 6th texture. The direction of $F_{\text{attracting}}$ from the 6th texture is same as the sliding direction, so the average friction forces are lower. When the tip slides to left, it must overcome $F_{\text{attracting}}$ in the opposite direction, and the tip need to break the connection at the same time. Therefore, the average friction forces for the even sliding numbers are higher.

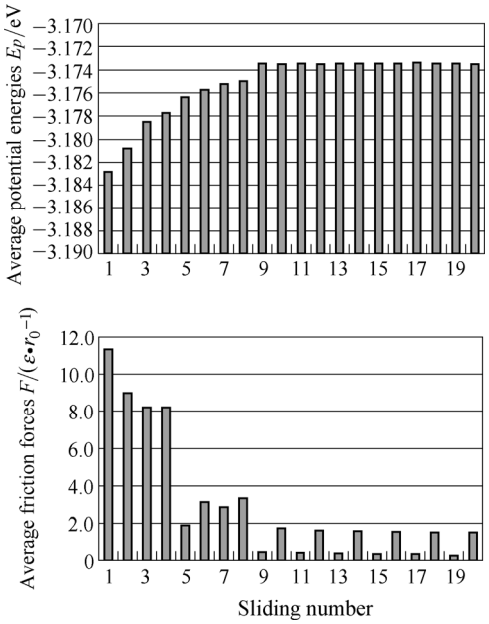


Fig. 6. Average potential energies and average friction forces for every sliding process (surface IV)

Similar to the cases of surfaces I and II, the average friction forces have a trend that they decrease as sliding numbers increase. Most textured surfaces in this work are rearranged during the sliding processes and induce lower average friction forces finally.

### 3.5 Discussion of the friction mechanism

For these four textured surfaces, when the sliding processes come to the final stage, the tip takes some atoms to slide on a big texture, and these big textures all contains two layers atoms. Besides, part of the surface of the tip is covered by one layer atoms. This phenomenon is caused by the indentation depth $d$, the radius of the tip $R$ and the structure of these textured surfaces. When the indentation process finishes, the tip would be located at the position where the bottom layer of the tip and the topmost layer of the 4th texture overlap if we do not consider the movements of the substrate atoms, as shown in Fig. 7(a) (we choose surface III for an example here). Actually, the overlap phenomenon can not happen, instead the 4th texture is compressed as shown in Fig. 7(b). At the beginning of the sliding process, the tip takes some atoms to slide together or scratches some atoms to fill into the right spacing. Furthermore, some atoms will adhere to the tip and form one layer atoms to cover the surface of the tip finally, which is shown in Fig. 7(c). As the sliding going on, the spacing between the 4th and 5th textures is filled to be a flat texture with two layers atoms. Then a big texture which includes the filled spacing and the bottom two layers of the 4th and 5th textures is formed as shown in Fig. 7(c). The formation of the big texture should be a necessary condition that the sliding processes reach steady state, because the distance between the tip and the adhered layer is $d_y$ in $y$ direction, and the distance between the adhered layer and the topmost layer of the current texture is also $d_y$ in $y$ direction. Therefore, the indentation depth $d$ is one of the factors that determine the height of the big texture and thereby the sliding process.

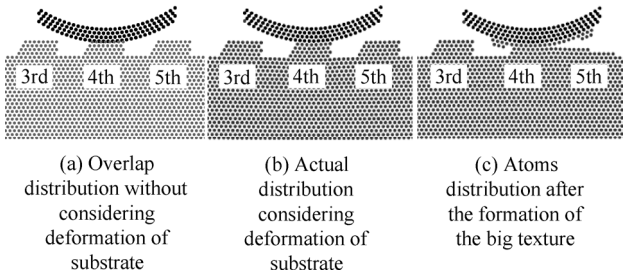


Fig. 7. Atoms distributions during the sliding process (surface III)

The radius of the tip $R$ is another factor which influences the sliding process. When the indentation finishes, the tip only interacts with the 4th texture, and the contact forces $F_N$ are shown in Fig. 8 (we also choose surface III for an example here). For the tip radius $R=30r_0$, contact forces on the surface of the 3rd and the 5th texture are all zero, so the tip only takes atoms from the 4th texture at the beginning of sliding process. In Ref. [22], when $R=100r_0$, the tip interacts with these 3 textures, and the friction forces and potential energies are all higher than the case of $R=30r_0$. Therefore, different tip radii will result in different sliding

processes, and the final structures of the big textures are also different.

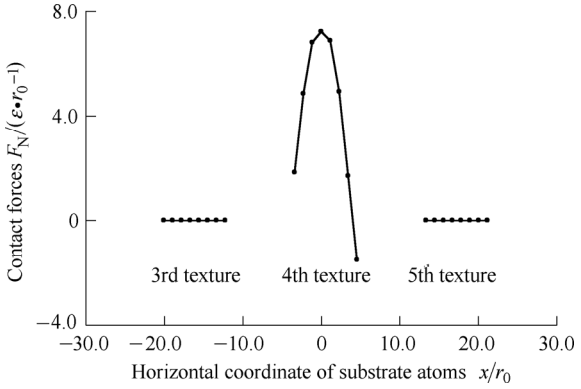


Fig. 8. Contact forces distribution on the three textures (surface III, $d$=2.5$r_0$)

The structures of the textured surfaces in this work help to form the big textures. The spacing between two textures is properly big enough, so the atoms scratched by the tip can fill the spacing and form a big flat texture during the sliding process.

Compared Figs. 5 and 6, one can find an interesting phenomenon that the average friction forces of textured surface III are much higher than the case of textured surface IV although a single texture of these two textured surfaces contains the same number of atoms. This phenomenon can be explained from the sliding processes: for the case of textured surface IV, when the sliding processes come to steady state, the atoms adhered to the tip are divided to two parts which are named as left part and right part. The left part does not contact with the big texture, and the force between the right part plays the main role, which causes lower average friction forces for textured surface IV. For textured surface III, the adhered atoms form a whole layer on the tip that interacts with the big texture, and more atoms' interactions produce higher average friction forces. The steady states of surfaces III and IV get the same trends that the average friction forces for the even sliding processes are higher than the case of odd sliding processes, which are caused by the attracting components $F_{\text{attracting}}$. The different behaviors of textured surfaces III and IV also indicate the important role of sliding direction.

In view of these, we can conclude that the reciprocating sliding contacts of textured surfaces are influenced by many factors, and a tiny variation of the textured surfaces can cause severe effects on the friction characteristics.

## 4 Conclusions

A study on two dimensional nanoscale reciprocating sliding contacts between a rigid cylindrical tip and an elastic substrate with textured surfaces is presented. Four textured surfaces with different texture shapes are designed. The average potential energies and average friction forces for these textured surfaces are investigated. The factors which influence the sliding processes are also discussed. Under the initial conditions and the textured surfaces chosen in this paper, some conclusions are drawn as follows.

(1) Textured surfaces influence the reciprocating sliding contacts characteristics significantly. For textured surfaces II, III and IV, the sliding processes come to the steady state, while textured surface I does not show stable sliding process in this study.

(2) Sliding direction will also affect the friction characteristics in reciprocating sliding contacts: the average potential energies get a single stable value as the sliding processes come to steady state, while the average friction forces are different for right and left sliding directions. Furthermore, the markedly different sliding contact behaviors between textured surfaces III and IV show the importance of sliding direction.

(3) Considering the different texture shapes in this work, if one wants to reduce friction forces and reach steady state quickly during the sliding process, textured surface IV should be a better choice.

(4) The indentation depth, the radius of the tip and the structures of textures will affect the sliding contact characteristics synthetically. These parameters determine the height of the big texture, the atoms adhered to the tip, and the number of textures which interact with the tip.

**References**

[1] RONEN A, ETSION I, KLIGERMAN Y. Friction-reducing surface-texturing in reciprocating automotive components[J]. *Tribology Transactions*, 2001,44(3): 359–366.

[2] RYK G, KLIGERMAN Y, ETSION I. Experimental investigation of laser surface texturing for reciprocating automotive components[J]. *Tribology Transactions*,2002, 45(4): 444–449.

[3] ETSION I. Improving tribological performance of mechanical components by laser surface texturing[J]. *Tribology Letters*, 2004, 17(4): 733–737.

[4] KLIGERMAN Y, ETSION I, SHINKARENKO A. Improving tribological performance of piston rings by partial surface texturing[J]. *ASME Journal of Tribology*, 2005, 127(3): 632–638.

[5] MITCHELL N, ELJACH C, LODGE B, et al. Single and reciprocal friction testing of micropatterned surfaces for orthopedic device design[J]. *Journal of the Mechanical Behavior of Biomedical Materials*, 2012, 7: 106–115.

[6] SINGH R A, YOON ES. Friction of chemically and topographically modified Si (1 0 0) surfaces[J]. *Wear*, 2007, 263(7): 912–919.

[7] MENEZES P L, KISHORE, KAILASS V, et al. The role of surface texture on friction and transfer layer formation during repeated sliding of Al-4Mg against steel[J]. *Wear*, 2011, 271(9–10): 1785–1793.

[8] GARRIDO A H, GONZÁLEZ R, CADENAS M, et al. Tribological behavior of laser-textured NiCrBSi coatings[J]. *Wear*, 2011, 271(5–6): 925–933.

[9] CHOUQUET C, GAVILLET J, DUCROS C, et al. Effect of DLC surface texturing on friction and wear during lubricated sliding[J]. *Materials Chemistry and Physics*, 2010, 123(2–3): 367–371.

[10] DENG J, SONG W, ZHANG H, et al. Friction and wear behaviors of the carbide tools embedded with solid lubricants in sliding wear tests and in dry cutting processes[J]. *Wear*, 2011, 270(9–10): 666–674.

[11] PODGORNIK B, VILHENA L M, SEDLAČEK M, et al.

Effectiveness and design of surface texturing for different lubrication regimes[J]. *Meccanica*, 2012, 47(7): 1613–1622.

[12] RAMESH A, AKRAM W, MISHRA S P, et al. Friction characteristics of microtextured surfaces under mixed and hydrodynamic lubrication[J]. *Tribology International*, 2013, 57: 170–176.

[13] KOVALCHENKO A, AJAYI O, ERDEMIR A, et al. Friction and wear behavior of laser textured surface under lubricated initial point contact[J]. *Wear*, 2011, 271(9–10): 1719–1725.

[14] ACHANTA S, DREES D, CELIS J P. Friction and nanowear of hard coatings in reciprocating sliding at milli-Newton loads[J]. *Wear*, 2005, 259(1–6): 719–729.

[15] PETTERSSON U, JACOBSON S. Textured surfaces for improved lubrication at high pressure and low sliding speed of roller/piston in hydraulic motors[J]. *Tribology International*, 2007, 40(2): 355–359.

[16] SPIJKER P, ANCIAUX G, MOLINARI J F. Dry sliding contact between rough surfaces at the atomistic scale[J]. *Tribology Letters*, 2011, 44(2): 279–285.

[17] QI Y, CHENG Y T, ÇAĞIN T, et al. Friction anisotropy at Ni(100)/(100)interfaces: molecular dynamics studies[J]. *Physical Review B*, 2002, 66(8): 085420(1–7).

[18] ZHANG Q, QI Y, HECTOR L G, et al. Atomic simulations of kinetic friction and its velocity dependence at Al/Al and $\alpha$-$Al_2O_3$/$\alpha$-$Al_2O_3$ interfaces[J]. *Physical Review B*, 2005, 72(4): 045406(1–12).

[19] HARRISON J A, COLTON R J, WHITE C T, et al. Effect of atomic-scale surface roughness on friction: a molecular dynamics study of diamond surfaces[J]. *Wear*, 1993, 168(1–2): 127–133.

[20] LUAN B Q, ROBBINS M O. Hybrid atomistic/continuum study of contact and friction between rough solids[J]. *Tribology Letters*, 2009, 36(1): 1–16.

[21] JENG Y R, TSAI P C, FANG T H. Molecular dynamics studies of atomic-scale tribological characteristics for different sliding systems[J]. *Tribology Letters*, 2005, 18(3): 315–330.

[22] TONG R T, LIU G, LIU T X. Multiscale analysis on two dimensional nanoscale sliding contacts of textured surfaces[J]. *ASME Journal of Tribology*, 2011, 133(4): 041401(1–13).

[23] HARRISON J A, WHITE C T, COLTON R J, et al. Molecular-dynamics simulations of atomic-scale friction of diamond surfaces[J]. *Physical Review B*, 1992, 46(15): 9700–9708.

[24] CHANDROSS M, LORENZ CD, STEVENSMJ, et al. Simulations of nanotribology with realistic probe tip models[J]. *Langmuir*, 2008, 24(4): 1240–1246.

[25] YUE L, ZHANG H, LI D Y. Defect generation in nano-twinned, nano-grained and single crystal Cu systems caused by wear: a molecular dynamics study[J]. *Scripta Materialia*, 2010, 63(11): 1116–1119.

[26] ZHU P Z, HU Y Z, WANG H. Molecular dynamics simulations of atomic-scale friction in diamond-silver sliding system[J]. *Chinese Science Bulletin*, 2009, 54(24): 4555–4559.

[27] LUAN B Q, HYUN S, MOLINARI J F. et al. Multiscale modeling of two-dimensional contacts[J]. *Physical Review E*, 2006, 74(4): 046710(1–11).

[28] PANDURANGAN V, NG T, LI H. Nanoscratch simulation on a copper thin film using a novel multiscale model[J]. *Journal of Nanomechanics and Micromechanics*, 2013, 10.1061/(ASCE)NM.2153-5477.0000084: A4013008(1–8).

[29] AGRAWAL P M, RICE B M, THOMPSON D L. Predicting trends in rate parameters for self-diffusion on FCC metal surfaces[J]. *Surface Science*, 2002, 515(1): 21–35.

[30] DOLL J D, MCDOWELL H K. Theoretical studies of surface diffusion: self-diffusion in the FCC (111) system[J]. *The Journal of Chemical Physics*, 1982, 77(1): 479–483.

[31] SWOPE W C, ANDERSEN H C, BERENS P H, et al. A computer simulation method for the calculation of equilibrium constants for the formation of physical clusters of molecules: application to small water clusters[J]. *The Journal of Chemical Physics*, 1982, 76(1): 637–649.

[32] YANG J, KOMVOPOULOS K. A molecular dynamics analysis of surface interference and tip shape and size effects on atomic-scale friction[J]. *ASME Journal of Tribology*, 2005, 127(3): 513–521.

[33] MOORE D F. *Principles and applications of tribology*[M]. Oxford: Pergamon Press, 1975.

## Biographical notes

TONG Ruiting, born in 1981, is currently an associate professor at *Northwestern Polytechnical University, China*. His research interests include multiscale method, contact mechanics, nanoscale friction, etc.
Tel: +86-13519151977; E-mail: tongruiting@nwpu.edu.cn

LIU Geng, born in 1961, is currently a professor at *Northwestern Polytechnical University, China*. His research interests include dynamics of mechanical system, tribology, contact mechanics, biomechanics, multiscale method, etc.
E-mail: npuliug@nwpu.edu.cn

LIU Tianxiang, born in 1976, is currently are search fellow at *Institute of Mechanics and Fluid Dynamics, TU Bergakademie Freiberg, Germany*. His research interests include mesh free method, contact mechanics, nanoscale friction, etc.
E-mail: tianxiang.liu@imfd.tu-freiberg.de